Supplementary Information

Additional file 2: Supplementary Materials for: Integrated Analyses of Multi-omic Data Derived from Paired Primary Lung Cancer and Brain Metastasis Reveal the Metabolic Vulnerability as a Novel Therapeutic Target. This file includes Supplementary Figures: Fig. S1-S8

Fig. S1: Analysis pipeline for integrated multi-omics data in this study.
Fig. S2: Mutation landscape in paired primary lung cancer and brain metastases.
Fig. S3: Comparative tumor mutational burden in lung cancer and brain metastases.
Fig. S4: Copy number alterations in primary lung cancer versus brain metastases.
Fig. S5: Principal component analysis and pathway enrichment in lung cancer brain metastasis.
Fig. S6: Immune pathway correlations and lymphocyte composition in lung cancer brain metastases.
Fig. S7: Enrichment analysis of mitochondrial and immune pathways in independent brain metastasis cohort.
Fig. S8: Immunohistochemical profiling of proliferation and immune markers in brain metastases.

Supplemental Figure 1

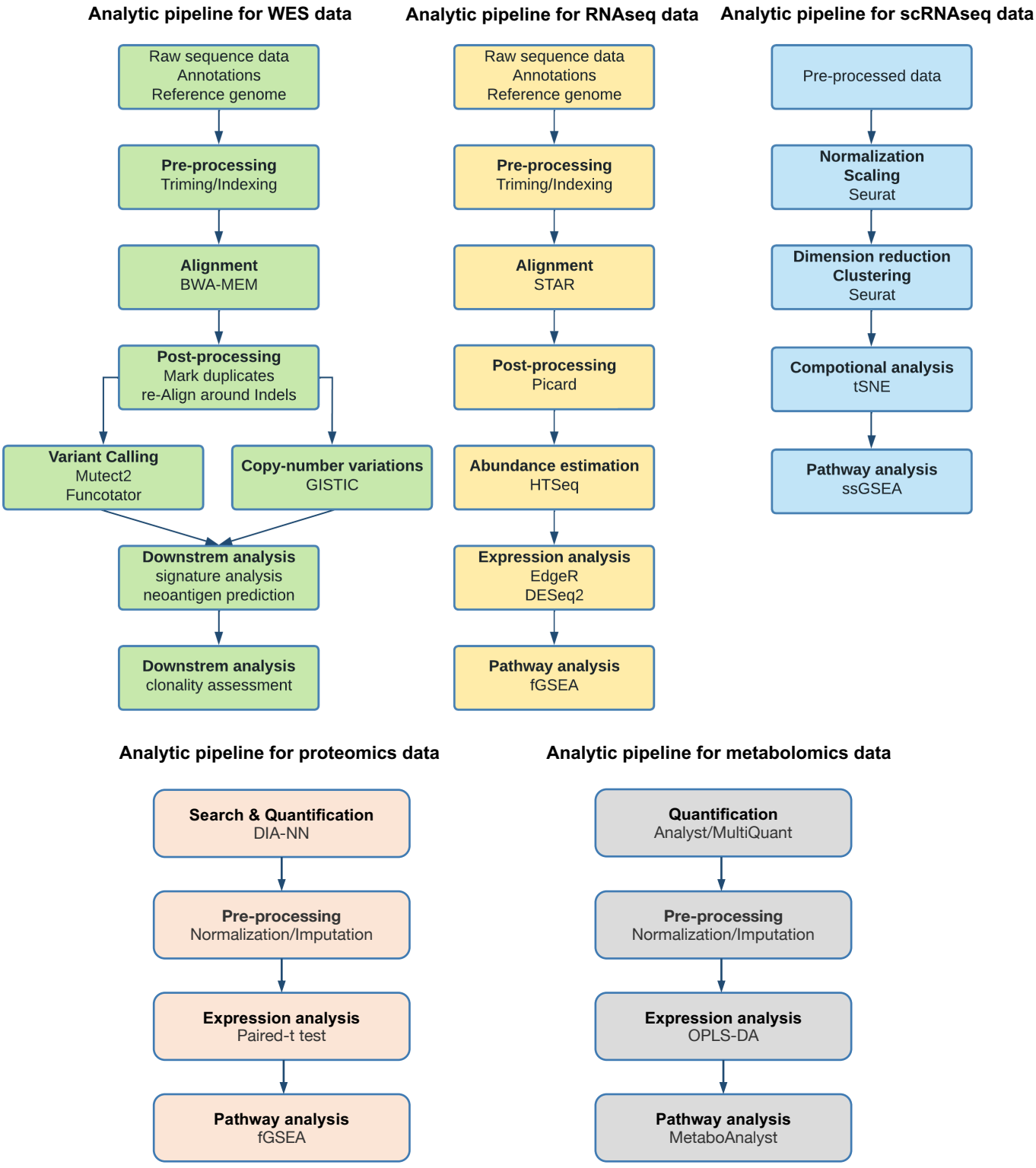

Fig. S1. Related to Figure 1. Analysis pipeline for integrated multi-omics data in this study. Analysis pipeline for whole-exome sequencing (WES), RNA sequencing (RNAseq), single cell RNA sequencing (scRNAseq), proteomics, and metabolomics data. Flow-chart demonstrates sequential use of tools in evaluation of DNA, RNA, single cell RNA, protein and metabolite samples.

Supplemental Figure 2

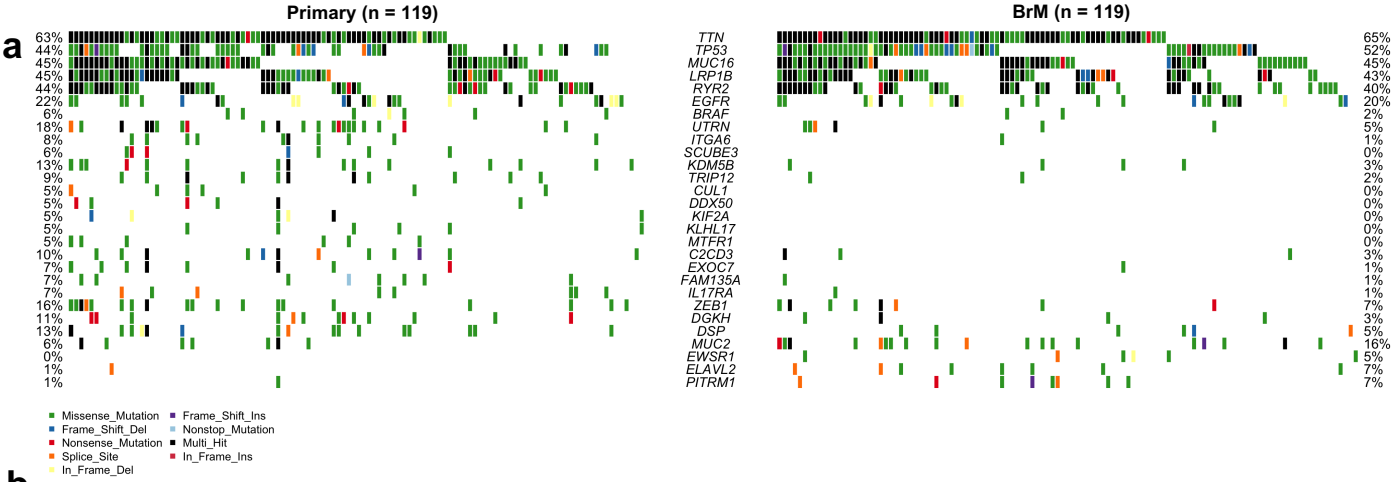

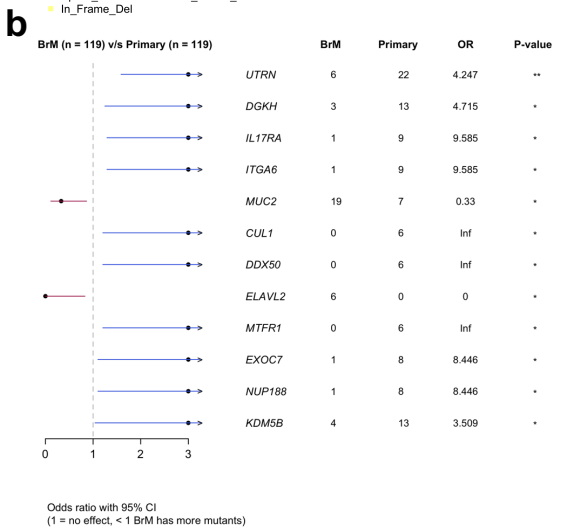

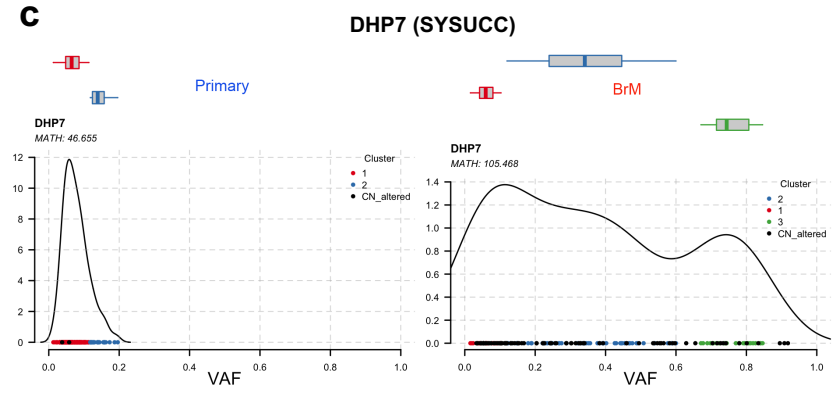

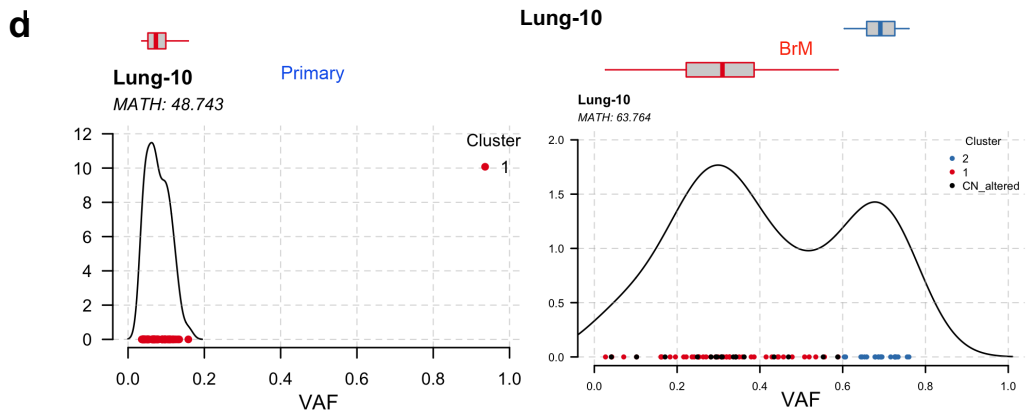

Fig. S2. Related to Figure 2. Mutation landscape in paired primary lung cancer and brain metastases. a. Oncoplot showing the specifically mutated genes in paired primary lung cancer and lung cancer brain metastasis (LC-BrM) specimens. **b.** Forrest plot to show the specifically mutated genes comparison in paired primary lung cancer and LC-BrM tumor specimens. **c and d.** Cluster plots of the primary lung cancer (left) and LC-BrM sample (right) derived from patient DHP7 and Lung-10. X-axis represented variant allele frequency, the top bar showed the number of clusters on top of each plot, and the MATH number was noted in the upper left corner.

Supplemental Figure 3

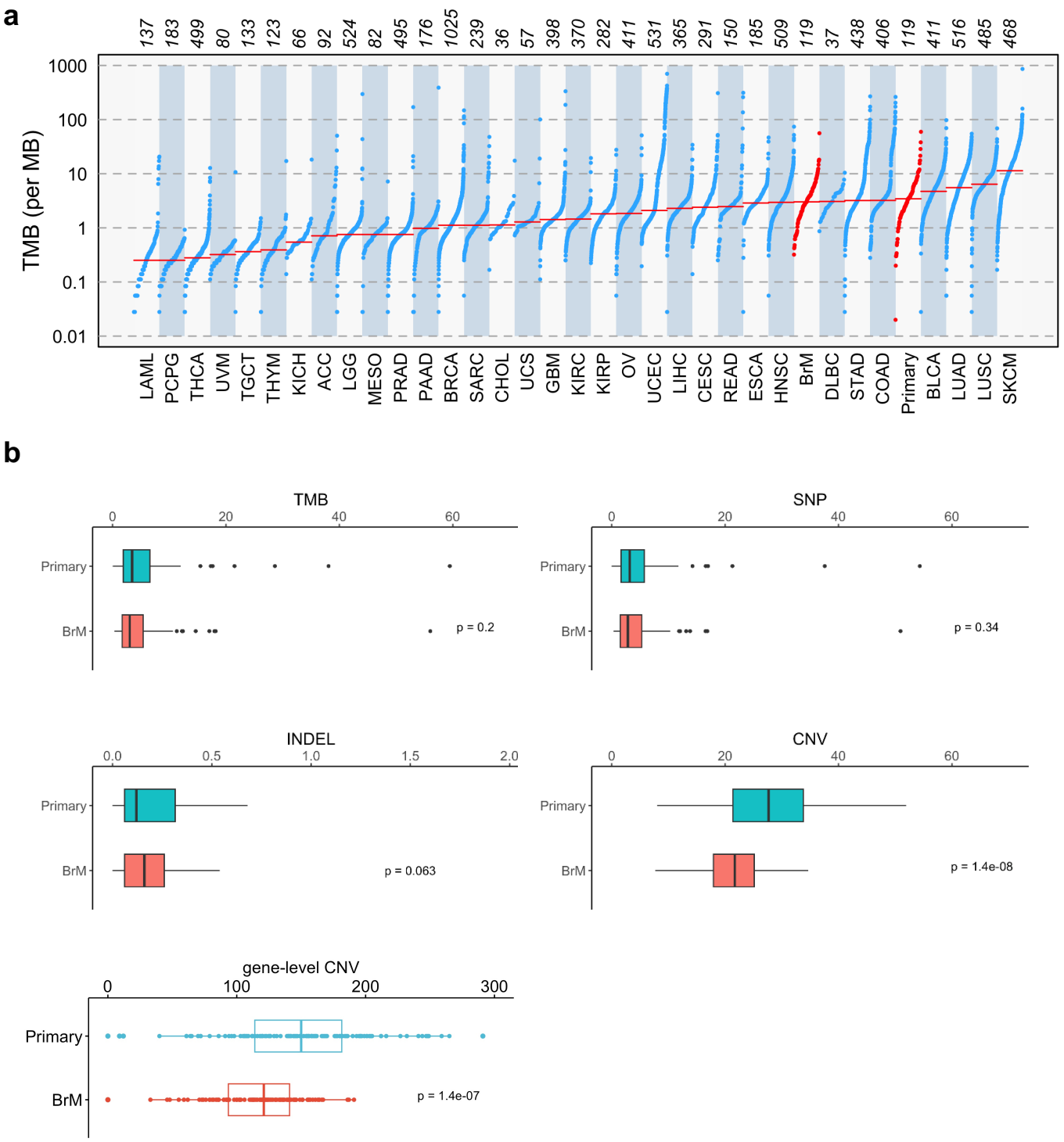

Fig. S3. Related to Figure 3. Comparative tumor mutational burden in lung cancer and brain metastases. a. Tumor mutation load comparison in primary, brain metastasis (BrM) against 33 TCGA cohorts derived from MC3 project. Top annotation is number of samples in each cohort, and y-axis is the logscale of tumor mutational burden with median mutation marked with red horizontal line. **b**. Box plots to show mutational burden comparison in matched primary lung cancer and BrM. The p-value was determined using pairwise two-sided Wilcoxon test.

Supplemental Figure 4

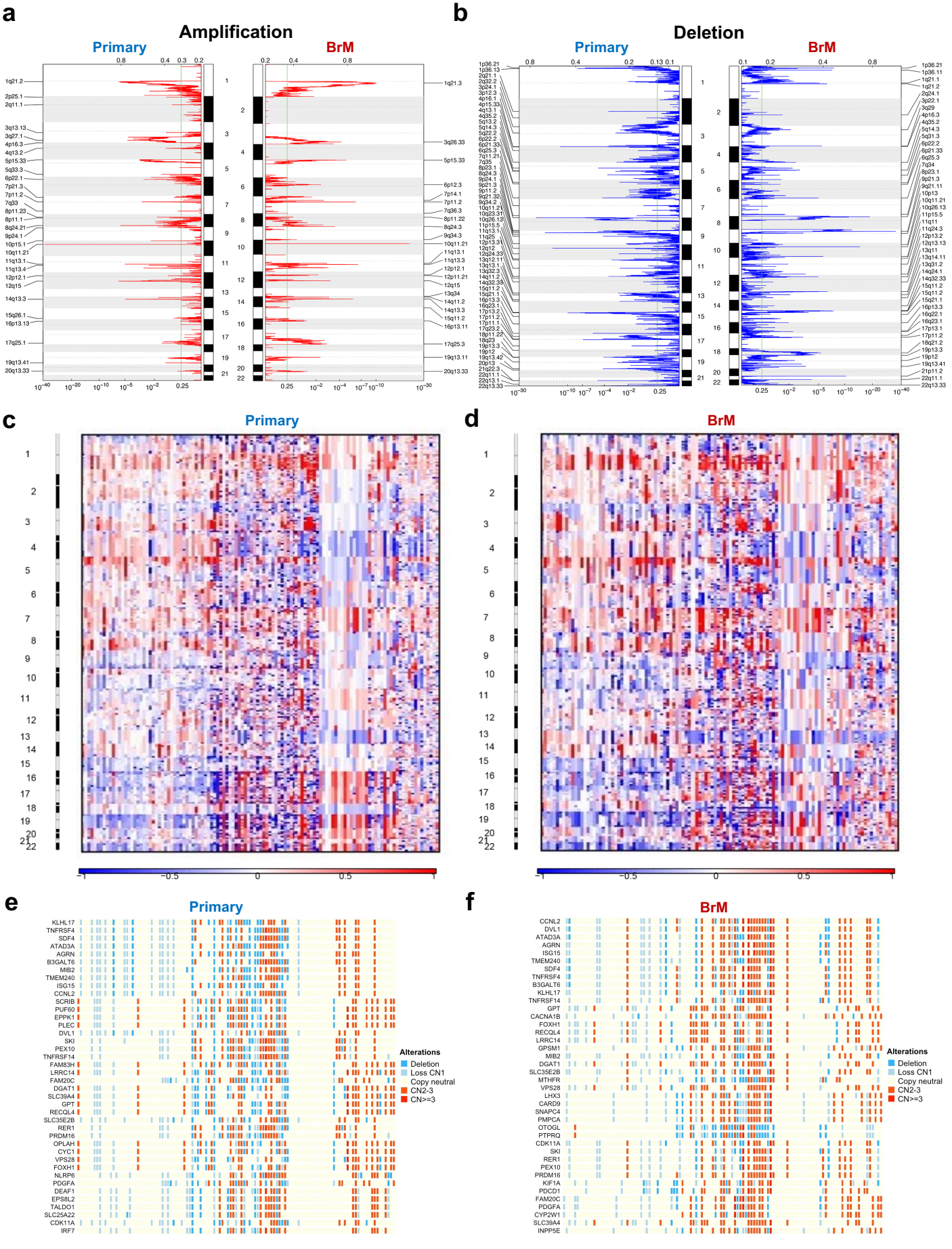

Fig. S4. Related to Figure 4. Copy number alterations in primary lung cancer versus brain metastases. **a and b.** Copy number gain (**a**) or loss (**b**) on the primary lung cancer (left column) and matched brain metastasis (BrM) samples (right column). **c and d**. Heatmap of copy number profiles for samples from primary lung cancer (**c**) and BrMs (**d**). Each row represents the copy number profile of a tumor sample across chromosomes 1 to 22 and X. Red indicates copy number gain; blue, loss. e and f. Specific genes of copy number gain and loss in primary lung cancer (**e**) and BrMs (**f**). Red indicates copy number gain (CN >= 3, CN2-3); yellow, no change (copy neutral); blue, loss (Deletion, Loss CN1).

Supplemental Figure 5

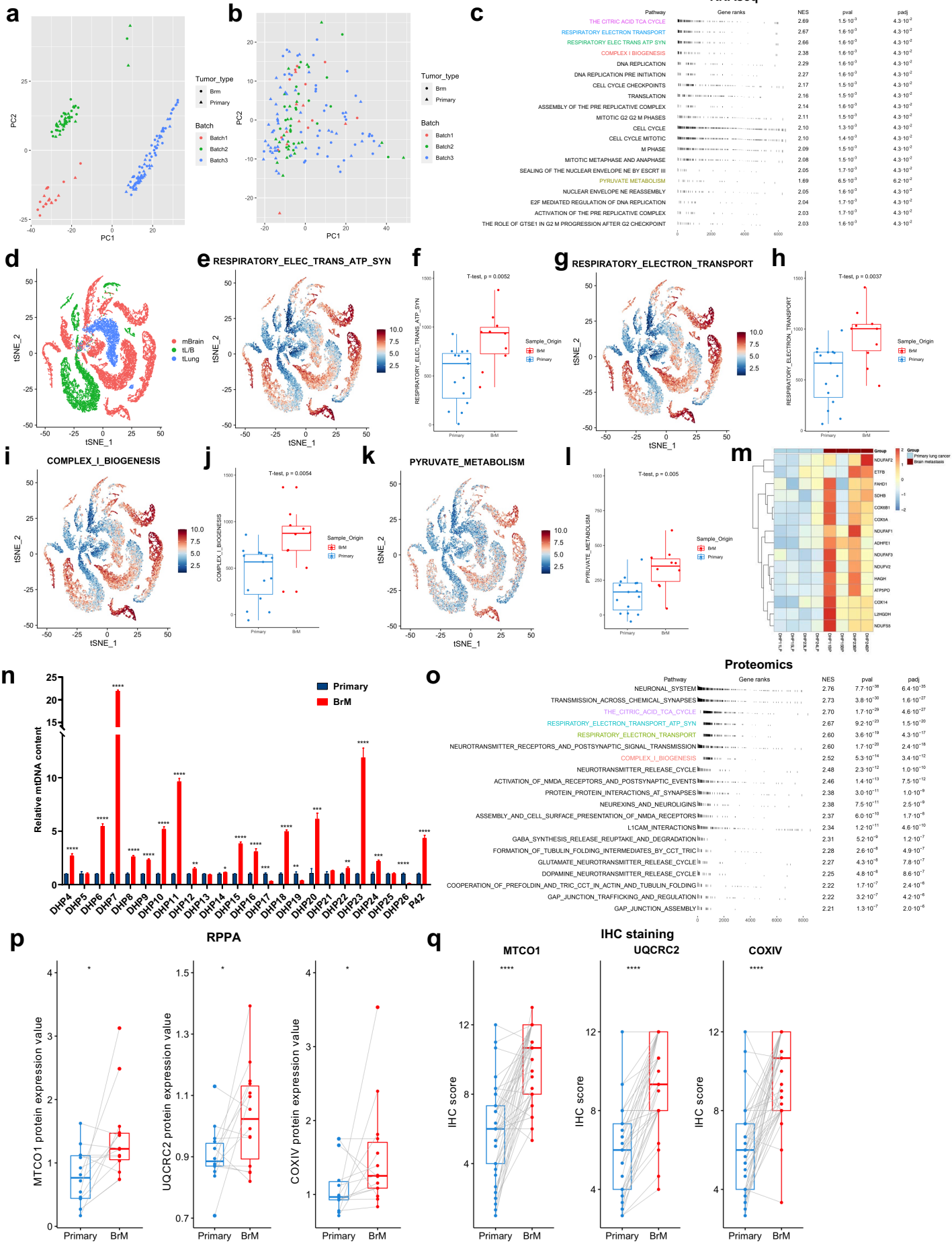

Fig. S5. Related to Figure 5. Principal component analysis and pathway enrichment in lung cancer brain metastasis. a and b. PCA plots to show the distribution of samples from two cohorts of 56 patients before (**a**) and after (**b**) ComBat process. **c.** The table of top 20 ranked gene pathways that were positively correlated with the lung cancer brain metastasis (LC-BrM) phenotype. Pathways were ordered by p-value and normalized enrichment score (NES). Five pathways related to mitochondrial biogenesis and oxidative phosphorylation were highlighted with different colors. **d.** tSNE plot of ~20,000 single epithelial cells with color-coded by three major cell lineages: 15,463 brain metastasis (mbrain) single cells, 7,270 early primary lung cancer (tLung) single cells and 6582 advanced-stage lung cancer (tL/B) single cells. **e-l**. tSNE plots and box plots of enrichment score of single epithelialcells for the rest four mitochondrial pathways mentioned in Figure 5b. **m.** the heatmap showing differentially expressed proteins related to mitochondrial biogenesis as identified in LC-BrMs in comparison with paired primary lung cancers. **n**. Relative mitochondrial DNA (mtDNA) content of paired primary lung cancer and brain metastasis lesions. The p-value was determined using pairwise two-sided Student's t test. **o.** The table of top 20 ranked protein pathways that were positively correlated with the LC-BrM phenotype. Pathways were ordered by p-value and NES. Four pathways related to mitochondrial biogenesis and oxidative phosphorylation were highlighted with different colors. **p.** Box plots showing the protein expression of MTCO1, UQCRC2 and COXIV based on reverse phase protein array data in nine paires of primary lung and brain metastasis lesions. The p-value was determined using pairwise two-sided Student's t test. **q.** Box plots for the immunohistochemistry scores of MTCO1, UQCRC2 and COXIV in 51 paires of primary lung and brain metastatic lesions. The p-value is determined using pairwise two-sided Student's t test. *, $p<0.05$; **, $p<0.01$; ***, $p<0.001$; ****, $p<0.0001$.

Supplemental Figure 6

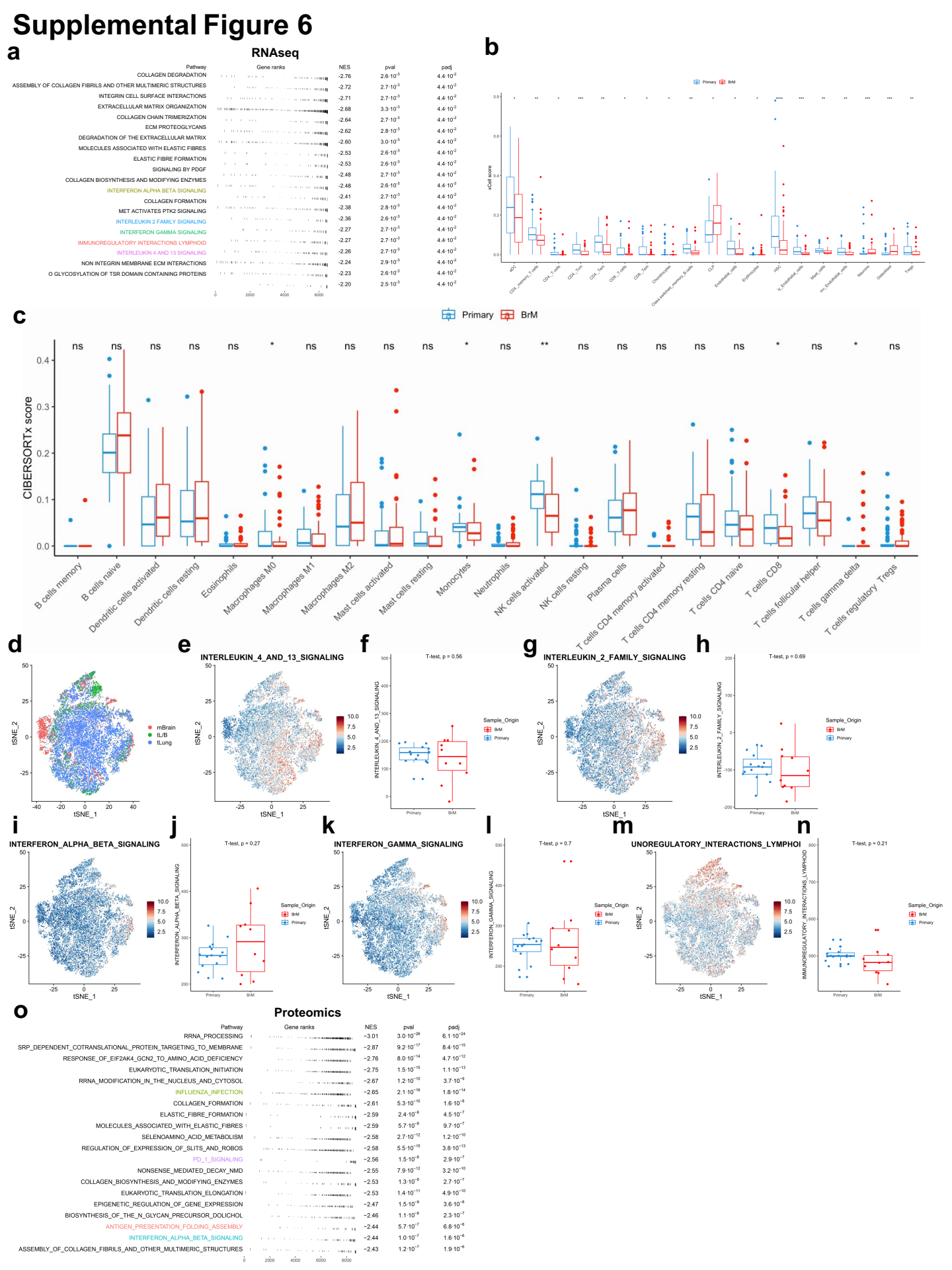

o

Proteomics

Pathway	Gene ranks	NES	pval	padj
RRNA_PROCESSING		−3.01	$3.0 \cdot 10^{-26}$	$6.1 \cdot 10^{-24}$
SRP_DEPENDENT_COTRANSLATIONAL_PROTEIN_TARGETING_TO_MEMBRANE		−2.87	$9.2 \cdot 10^{-17}$	$8.4 \cdot 10^{-15}$
RESPONSE_OF_EIF2AK4_GCN2_TO_AMINO_ACID_DEFICIENCY		−2.76	$8.0 \cdot 10^{-14}$	$4.7 \cdot 10^{-12}$
EUKARYOTIC_TRANSLATION_INITIATION		−2.75	$1.5 \cdot 10^{-15}$	$1.1 \cdot 10^{-13}$
RRNA_MODIFICATION_IN_THE_NUCLEUS_AND_CYTOSOL		−2.67	$1.2 \cdot 10^{-10}$	$3.7 \cdot 10^{-9}$
INFLUENZA_INFECTION		−2.65	$2.1 \cdot 10^{-16}$	$1.8 \cdot 10^{-14}$
COLLAGEN_FORMATION		−2.61	$5.3 \cdot 10^{-10}$	$1.6 \cdot 10^{-8}$
ELASTIC_FIBRE_FORMATION		−2.59	$2.4 \cdot 10^{-8}$	$4.5 \cdot 10^{-7}$
MOLECULES_ASSOCIATED_WITH_ELASTIC_FIBRES		−2.59	$5.7 \cdot 10^{-8}$	$9.7 \cdot 10^{-7}$
SELENOAMINO_ACID_METABOLISM		−2.58	$2.7 \cdot 10^{-12}$	$1.2 \cdot 10^{-10}$
REGULATION_OF_EXPRESSION_OF_SLITS_AND_ROBOS		−2.58	$5.5 \cdot 10^{-15}$	$3.8 \cdot 10^{-13}$
PD_1_SIGNALING		−2.56	$1.5 \cdot 10^{-6}$	$2.9 \cdot 10^{-7}$
NONSENSE_MEDIATED_DECAY_NMD		−2.55	$7.9 \cdot 10^{-12}$	$3.2 \cdot 10^{-10}$
COLLAGEN_BIOSYNTHESIS_AND_MODIFYING_ENZYMES		−2.53	$1.3 \cdot 10^{-8}$	$2.7 \cdot 10^{-7}$
EUKARYOTIC_TRANSLATION_ELONGATION		−2.53	$1.4 \cdot 10^{-11}$	$4.9 \cdot 10^{-10}$
EPIGENETIC_REGULATION_OF_GENE_EXPRESSION		−2.47	$1.5 \cdot 10^{-9}$	$3.6 \cdot 10^{-8}$
BIOSYNTHESIS_OF_THE_N_GLYCAN_PRECURSOR_DOLICHOL		−2.46	$1.1 \cdot 10^{-8}$	$2.3 \cdot 10^{-7}$
ANTIGEN_PRESENTATION_FOLDING_ASSEMBLY		−2.44	$5.7 \cdot 10^{-7}$	$6.8 \cdot 10^{-6}$
INTERFERON_ALPHA_BETA_SIGNALING		−2.44	$1.0 \cdot 10^{-7}$	$1.6 \cdot 10^{-6}$
ASSEMBLY_OF_COLLAGEN_FIBRILS_AND_OTHER_MULTIMERIC_STRUCTURES		−2.43	$1.2 \cdot 10^{-7}$	$1.9 \cdot 10^{-6}$

Fig. S6. Related to Figure 6. Immune pathway correlations and lymphocyte composition in lung cancer brain metastases. a. The table of bottom 20 ranked gene pathways that were negatively correlated with the phenotype of lung cancer brain metastasis (LC-BrM). Pathways were ordered by p-value and normalized enrichment score (NES). Five immune related pathways were highlighted with different colors. **b and c.** Box plot representation of xCell (**b**) and CIBERSORTx (**c**) scores for patients with paired primary lung cancer and LC-BrMs. The p-value was determined by use of pairwise t-test. **d.** tSNE plot of ~20,000 lymphocytes with color-coded by three major cell lineages: 3910 brain metastasis (mbrain) single cells, 18587 early primary lung cancer (tLung) single cells, and 3627 advanced-stage lung cancer (tL/B) single cells. **e-n.** tSNE plots and box plots of enrichment score of single lymphocytes for the five immune pathways mentioned in Figure 6a. **o**. The table of bottom 20 ranked protein pathways that were negatively correlated with the phenotype of LC-BrM. Pathways were ordered by p-value and NES. Four immune related pathways were highlighted with different colors.

Supplemental Figure 7

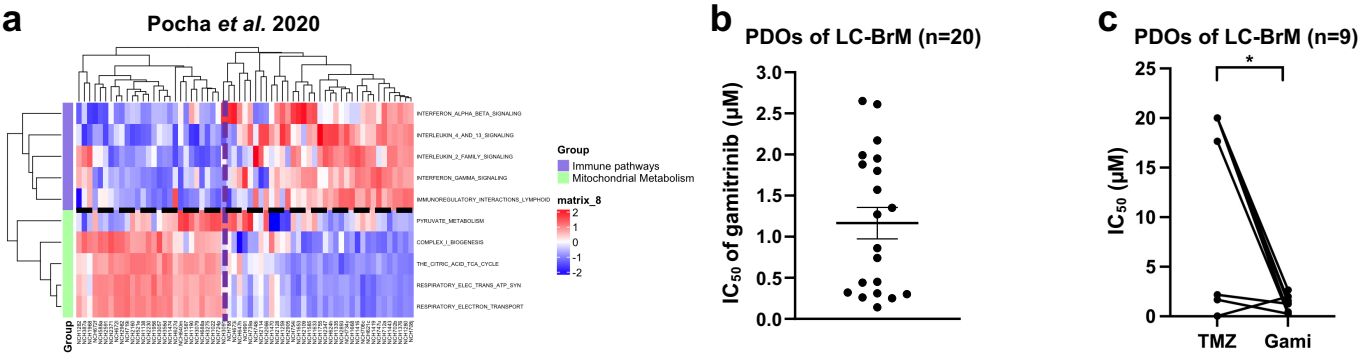

Fig. S7. Related to Figure 7. Enrichment analysis of mitochondrial and immune pathways in independent brain metastasis cohort. a. The heatmap showing the enrichment of indicated five mitochondrial pathways and five immune pathways in an independent cohort of 63 brain metastasis (BrM) lesions with mRNA microarray data. **b.** Scatter plot showing the IC_{50} to gamitrinib of 20 BrM patient-derived organoids (PDOs). **c.** Box plots showing the IC_{50} of temozolomide (TMZ) and gamitrinib in BrM PDOs. The p-value was determined using pairwise two-sided Wilcoxon test. *, $p<0.05$.

Supplemental Figure 8

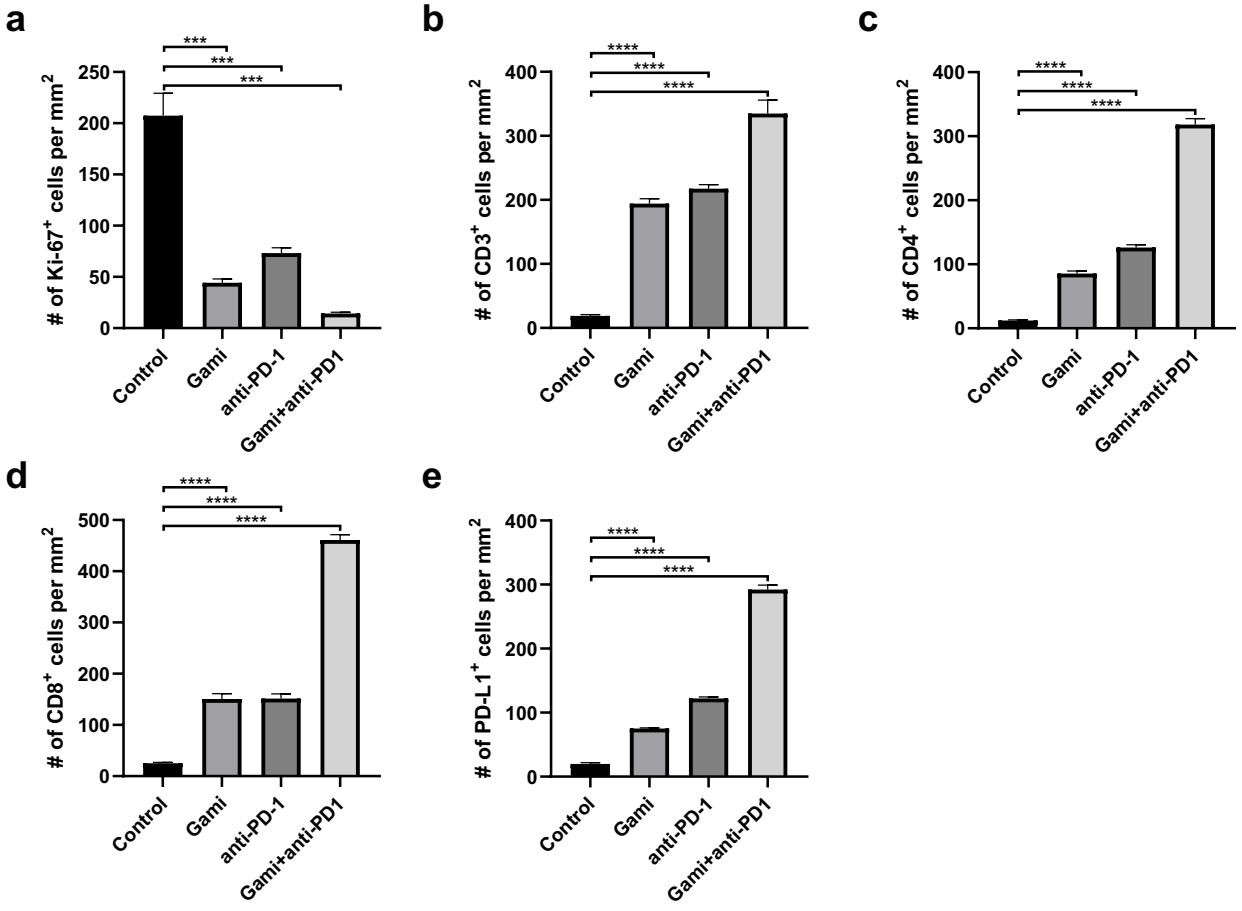

Fig. S8. Related to Figure 8. Immunohistochemical profiling of proliferation and immune markers in brain metastases. a-e. Bar plots of quantification analyses of immunohistochemistry staining of Ki-67 (**a**), CD3 (**b**), CD4 (**c**), CD8 (**d**), and PD-L1 (**e**) in Lewis lung carcinoma brain metastases. The p-value is determined using two-sided Student's t test. ***, $p<0.001$; ****, $p<0.0001$.